

Global auroral responses to abrupt solar wind changes: Dynamic pressure, substorm, and null events

L. R. Lyons,¹ D.-Y. Lee,² C.-P. Wang,¹ and S. B. Mende³

Received 17 February 2005; revised 18 February 2005; accepted 26 April 2005; published 25 August 2005.

[1] Global auroral images are used to investigate how specific types of solar wind change relate to the resulting type of auroral-region disturbance, with the goal of determining fundamental response types. For not strongly southward IMF conditions ($B_z \gtrsim -5$ nT), we find that IMF changes that are expected to reduce the convection electric field after $\gtrsim 30$ min of negative IMF B_z cause typical substorms, where expansion phase auroral activity initiates within the expected location of the Harang electric field reversal and expands in ~ 10 min to cover ~ 5 hours of MLT. For not strongly southward IMF conditions, solar wind dynamic pressure (P_{dyn}) enhancements compress the entire magnetosphere, leading to a global auroral enhancement with no evidence for substorm bulge-region aurora or current wedge formation. Following prolonged strongly southward IMF ($B_z \lesssim -8$ nT), an IMF change leading to convection electric field reduction gives a substorm disturbance that is not much different from substorms for less strongly southward IMF conditions, other than the expansion phase auroral bulge region seems to expand somewhat more in azimuth. However, under steady, strongly southward IMF conditions, a P_{dyn} enhancement is found to cause both compressive auroral brightening away from the bulge region and a Harang-region substorm auroral brightening. These two auroral enhancements merge together, leading to a very broad auroral enhancement covering ~ 10 – 15 hours of MLT. Both current wedge formation and compressive energization in the inner plasma sheet apparently occur for these events. We also find that interplay of effects from a simultaneous IMF and P_{dyn} change can prevent the occurrence of a substorm, leading to what we refer to as null events. Finally, we apply the plasma sheet continuity equation to the IMF and pressure driven substorm responses and the null events. This application suggests that solar wind changes cause substorm onset only if the changes lead to a reduction in the strength of convection within the inner plasma sheet.

Citation: Lyons, L. R., D.-Y. Lee, C.-P. Wang, and S. B. Mende (2005), Global auroral responses to abrupt solar wind changes: Dynamic pressure, substorm, and null events, *J. Geophys. Res.*, **110**, A08208, doi:10.1029/2005JA011089.

1. Introduction

[2] Abrupt solar wind changes can lead to important large-scale disturbances of the magnetosphere-ionosphere system that significantly affect the space environment, including energetic particle fluxes both in the magnetosphere and precipitating into the ionosphere as well as magnetospheric and ionospheric current systems. A fundamental aspect of understanding and predicting these disturbances is determining how to directly relate specific solar wind changes to the type, structure, and intensity of the

resulting disturbance. While much effort has been devoted to general correlations between solar wind parameters and measures of overall geomagnetic activity, most large-scale disturbances are related to specific solar wind changes and far less attention has been given to relating specific structures in the solar wind to the specific resulting disturbance. Two different types of such disturbance have so far been identified: substorms and what we will here refer to as “dynamic pressure disturbances.”

[3] It has been well established that interplanetary magnetic field (IMF) changes that lead to a reduction in the strength of large-scale convection, after a $\gtrsim 30$ min period of enhanced convection, lead to substorms. (It has not yet been possible to determine whether or not all substorm onsets are caused by such IMF changes; however, it has been shown that at least $\sim 60\%$ of substorms occur in this way [Lyons *et al.*, 1997, 2003a; Hsu and McPherron, 2002, 2003] and that substorms generally do not occur while the IMF and solar wind dynamic pressure are constant as occurs during convection bays as well as during the main phase of some magnetic storms [Zhou *et al.*, 2003; Tsurutani *et al.*, 2004]).

¹Department of Atmospheric and Oceanic Sciences, University of California, Los Angeles, California, USA.

²Department of Astronomy and Space Science, College of Natural Sciences and Institute for Basic Science Research, Chungbuk National University, Chungbuk, South Korea.

³Space Sciences Laboratory, University of California, Berkeley, California, USA.

Auroral activity during substorms typically initiates near the equatorward boundary of the auroral oval and within a ~ 1 – 2 hour MLT sector that is within the electric field reversal region known as the Harang discontinuity [Nielsen and Greenwald, 1978; Baumjohann *et al.*, 1981; Nielsen, 1991; Hughes and Bristow, 2003], which we refer to here as the “Harang reversal” since it is not a discontinuity. After onset, substorm auroral activity expands both poleward and azimuthally, leading to an “auroral bulge” that protrudes into the nightside polar cap. Generally, auroral activity remains confined to a several hour MLT range of the night side during the expansion phase of substorms. The substorm auroral enhancement is generally believed to be associated in MLT with current-wedge formation in the inner plasma sheet, the azimuthal expansion being associated [Gelpi *et al.*, 1987] with the well-known azimuthal expansion of the current wedge [Arnoldy and Moore, 1983; Nagai, 1987].

[4] More recently, solar wind dynamic pressure enhancements have been found to cause disturbances as important as substorms but with large-scale auroral and trapped radiation responses that are very different from those associated with substorms [e.g., Zesta *et al.*, 2000; Lyons *et al.*, 2000; Chua *et al.*, 2001; Boudouridis *et al.*, 2003]. During such disturbances, there is a rapid global enhancement of auroral emissions as well as a significant poleward motion of the poleward boundary of the aurora. These effects have been seen to initiate at nearly the same time as the dynamic pressure enhancement first impacts the magnetosphere, and they have been seen to occur nearly simultaneously over most of the auroral oval. Such global enhancement of the aurora cannot be related to an azimuthally localized current wedge and seems clearly to be a result of the global energization of magnetospheric particles by the compression of the magnetosphere that accompanies an enhancement in dynamic pressure.

[5] The above results show that there is a clear distinction between the physics of substorms, which are relatively localized in MLT extent and are related to the Harang reversal, and dynamic pressure disturbances, which appear to be a direct and global consequence of compression. However, as will be demonstrated in this paper, global auroral images from the IMAGE spacecraft show striking evidence that there are also important differences between these disturbances when they follow prolonged periods of strongly southward IMF and when they follow less extreme conditions. Furthermore, these images show strong evidence of an important interplay of effects that occurs when a solar wind change has both a significant IMF change and a significant dynamic pressure change. The identified interplay prevents the onset of a substorm disturbance, leading to what we here refer to as “null” events, and this interplay provides potentially important new information for understanding substorms and dynamic pressure disturbances.

[6] The primary data considered here are global auroral images from the Wideband Imaging Camera (WIC) on the IMAGE spacecraft, supporting information being obtained from low-latitude ground magnetic field measurements. In the companion paper [Lee *et al.*, 2005; hereinafter referred to as Paper 2] we consider the geosynchronous energetic particle and magnetic field responses to abrupt solar wind changes and put results in context with the different

responses seen in the global auroral images. We first focus on ideal events due to solar wind changes that have only an IMF or dynamic pressure change. We illustrate differences and similarities between IMF-driven substorms and dynamic pressure disturbances under typical IMF conditions (i.e., not following prolonged strongly southward IMF), and then evaluate differences and similarities between those disturbances that occur following periods of strongly southward IMF and those that do not. Next we show examples where the interplay between IMF and pressure change effects leads to null events.

2. Not Strongly Southward IMF Conditions

2.1. Northward Turning Substorms

[7] It is well known that IMF changes that lead to a convection reduction after a ≥ 30 min period of negative B_z lead to the onset of substorms. The upper panels of Figure 1 shows the IMF B_z and solar wind dynamic pressure P_{dyn} as observed by the ACE and Geotail spacecraft within the solar wind for a period including one such substorm with onset at ~ 1914 UT on 9 December 2000. ACE was about 1 hour upstream of the Earth and observed an IMF northward turning at 1807 UT that followed a ~ 30 min period of mostly southward IMF from -2 to -4 nT. Geotail, much nearer the Earth, observed this northward turning at 1911 UT following an ~ 25 min period of $B_z \sim -3$ nT. The detailed structure of the IMF is different between the two spacecraft. However, a northward turning following an ~ 30 min period of southward IMF was observed by both spacecraft with a time difference appropriate for their spatial separation. Both spacecraft show that there were no significant changes in P_{dyn} near the time of the northward turning. Also, the two spacecraft were on opposite sides of Earth, ACE being on the duskside and Geotail on the dawnside. It thus seems quite clear that this IMF northward turning with approximately constant P_{dyn} impacted the magnetosphere within several minutes of the time it was observed at Geotail.

[8] The middle panels of Figure 1 show the magnetic H-component from six low-latitude ground stations distributed in longitude around the Earth. These data show a nightside positive perturbation at BNG and ABG, initiating near 1915 UT at ABG, as is associated with substorm current wedge formation. No significant H-component changes are observed on the dayside in association with this onset, as expected if the P_{dyn} impacting the magnetosphere was approximately constant. The lower panels of Figure 1 show magnetic field data from the Goes 8 and 10 geosynchronous spacecraft, located on the dayside on either side of noon at the time of the onset. These data show no changes associated with the onset, which is also consistent with a constant P_{dyn} impacting the magnetosphere.

[9] Global auroral images from WIC for this substorm event are shown in Figure 2a. WIC is part of the Far Ultraviolet Imager on board the IMAGE spacecraft. It was designed to image the aurora in a broadband (between 140 nm and 180 nm in the ultraviolet) for maximum spatial resolution and to image the whole Earth and the auroral oval from satellite radial distances greater than $4 R_E$. The temporal resolution between two images is 123 s, and the size of the final images is 256×256 pixel elements, which

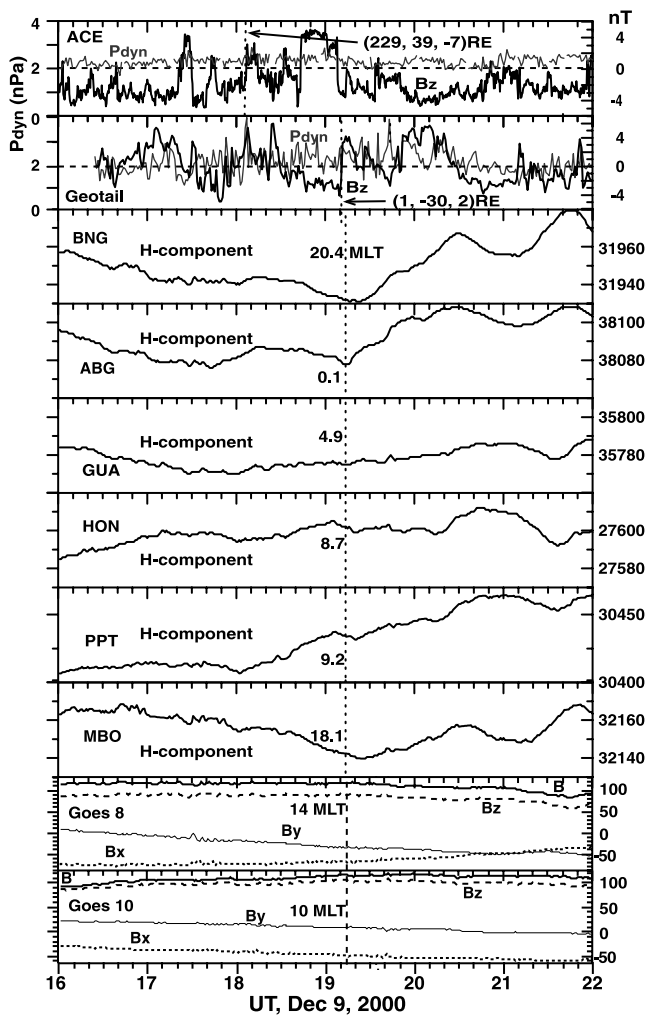


Figure 1. (top) IMF B_z and P_{dyn} as observed by the ACE and Geotail spacecraft within the solar wind, (middle) magnetic H-component from six low-latitude ground stations distributed in longitude around the Earth, and (bottom) magnetic field in GSM from the Goes 8 and 10 geosynchronous spacecraft for a northward turning substorm on 9 December 2000. The times of the IMF northward turning at each solar wind spacecraft and of its first effects on ground H-component are indicated by a vertical dashed line in each panel.

corresponds to spatial resolutions of less than 100 km at IMAGE apogee. WIC images are shown every 2 to 4 min in Figure 2a in an MLT-invariant latitude polar grid having midnight at the bottom and dusk to the left of each image. Latitude circles are shown every 10° , and the entire auroral oval can be seen in the images.

[10] The images in Figure 2a show that brightening within the equatorward portion of the oval was first visible at 1914 UT at ~ 0000 to 0100 MLT. Such brightening indicates the onset of a substorm expansion. On the basis of the previous studies referred to in section 1, this brightening, as well as other similar brightenings discussed later, occurs within the region of the Harang reversal. Different onsets occur at different nightside MLTs, as determined by

the location of the Harang reversal prior to onset [Gjerloev *et al.*, 2003].

[11] The region of enhanced expansion-phase aurora then spreads azimuthally and poleward over the next 4–6 min, forming a typical aurora bulge and reaching a maximum azimuthal coverage of ~ 5 hours of MLT. This expansion-phase bulge indicates that current-wedge formation occurred within the inner plasma sheet. Consistent with this, the geosynchronous energetic particle data for this event show the clear dispersionless flux enhancements near midnight that result from current wedge formation (see Paper 2 and references therein for examples of such dispersionless flux enhancements). Fading of the enhanced aurora is clear by 1922 UT, indicating that the substorm recovery phase was underway. Notice that there is no persistent auroral brightening away from the bulge region. These auroral features are typical of those seen in WIC images for substorms initiated by IMF driven reduction in convection without a significant change in P_{dyn} (such as the above northward IMF turning) following growth-phase periods of moderately southward IMF. We refer here to such substorms as “typical” substorms.

2.2. Dynamic Pressure Disturbances

[12] Figure 3 shows ACE and Geotail solar wind observations, the magnetic H-component from seven low-latitude ground stations distributed in longitude around the Earth, and the total magnetic field from the Goes 8 and 10 spacecraft for a P_{dyn} enhancement event on 11 August 2000. ACE and Geotail were on opposite sides of the Earth and indicate that an abrupt enhancement in P_{dyn} impacted the magnetosphere several minutes after 1840 UT. P_{dyn} more than doubled for this event, and the IMF B_z was near zero (Geotail) or slightly negative (ACE) and remained approximate constant during the event. The impact of this increase in P_{dyn} on the magnetosphere at 1847 UT shows clearly as an abrupt increase in the low-latitude H-component at all MLT and in the dayside geosynchronous magnetic field observed by the Goes spacecraft.

[13] Figure 4 shows the solar wind, low-latitude H (from two dayside stations), and Goes 8 and 10 total B and B_z observations for another large and abrupt increase in P_{dyn} that impacted the Earth at 1856 UT on 26 July 2000. For this case, P_{dyn} also more than doubled and the moderately negative IMF B_z before the event (-3 nT at ACE, -5 nT at Geotail) turned somewhat further negative (by ~ 4 nT at ACE, ~ 1.5 nT at Geotail) when P_{dyn} increased.

[14] WIC images for the above two pressure events are shown in Figures 2b and 2c, respectively. For these events, an enhancement of auroral emissions is observed over a wide range of MLT, both on the dayside and nightside. This enhancement is first clearly seen in the 1848:22 UT image on 11 August 2000 and the 1857:09 UT image on 26 July 2000. This is as close to simultaneous with the pressure impact as can be determined with the 2-min time resolution of WIC. Also note that unlike for typical substorms, for these events there is no evidence for bulge formation or for initiation of recovery of the enhanced emission to predisturbance levels within the 20 min period after onset for which images are shown in Figures 2b and 2c. Such a global auroral enhancement, without the bulge formation associated with current wedge formation, is the well-docu-

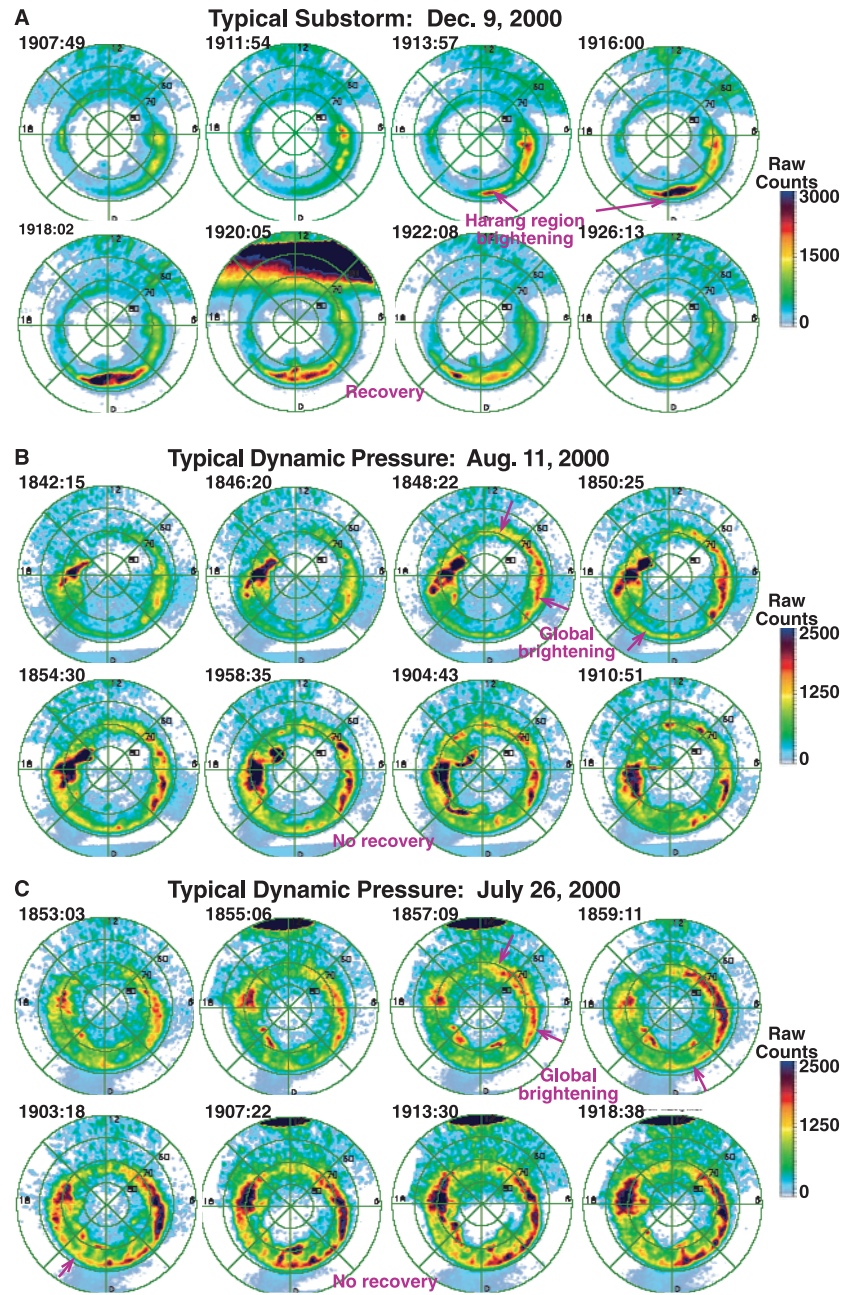


Figure 2. Selected global auroral images from WIC for a northward turning substorm with onset at ~ 1914 UT on 9 December 2000 and for dynamic pressure disturbances with onsets at ~ 1848 UT on 11 August 2000 and at 1857 UT on 26 July 2000.

mented response to solar wind dynamic pressure enhancements mentioned in section 1. Direct evidence for a lack of current wedge formation during this type of event has been found using geosynchronous observations by *Lee and Lyons* [2004].

[15] The auroral and geosynchronous response for these events is as expected from the magnetospheric compression resulting from an enhancement in P_{dyn} . Such compression globally increases the equatorial magnetic field and adiabatically energizes all trapped particles, including those undergoing strong pitch-angle diffusion throughout the aurora oval. We attribute most of the global auroral

enhancement to this enhancement of the diffuse aurora, though some discrete auroral features will also be enhanced due to the increase in the global field-aligned current system that has been observed in response to an increase in P_{dyn} . Here we refer to disturbances such as those shown in Figure 2b and 2c as “typical” dynamic pressure disturbances.

3. Strongly Southward IMF Conditions

[16] The characteristics of typical substorm and dynamic pressure disturbances discussed above are quite well known. However, these characteristics for moderate south-

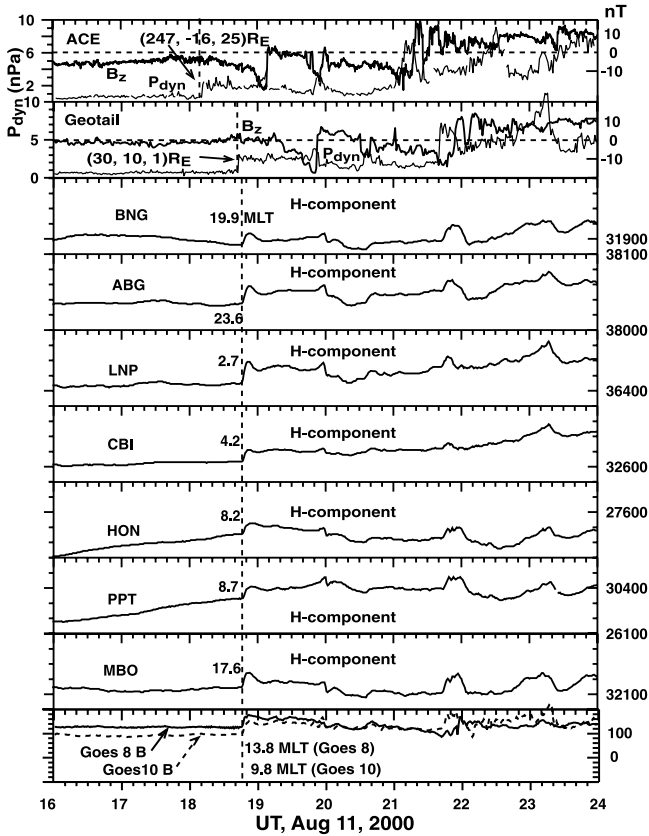


Figure 3. IMF B_z and P_{dyn} from ACE and Geotail, H-component from seven low-latitude ground stations distributed in longitude around the Earth, and the total B from the Goes 8 and 10 spacecraft for a P_{dyn} enhancement event on 11 August 2000. The times of the P_{dyn} enhancement at each solar wind spacecraft and of its first effects on the ground H-component are indicated by a vertical dashed line in each panel.

ward IMF conditions have not previously been directly compared to disturbances that occur following prolonged periods of strongly southward IMF conditions.

3.1. Northward Turning Substorms

[17] To investigate northward IMF turning substorms under strongly southward IMF conditions, we look at two events that occurred on 11 August 2000. Figure 5 shows ACE and Geotail solar wind observations and the magnetic H-component from four representative low-latitude ground stations distributed in longitude for 0000–1200 UT on 11 August 2000. The H traces are shown as heavy solid lines when the observing station was on the dayside and by a dotted line when the station was on the nightside. Geotail was unusually well located for this event, being almost directly in front of the noon magnetopause. This time period includes several good examples of IMF and P_{dyn} changes under strongly southward IMF conditions, identified by vertical dashed lines in the figure.

[18] The events labeled S1 and S2 in Figure 5 are IMF northward turnings events that followed ≥ 45 min intervals of $B_z \lesssim -6$ nT (Geotail) to -9 nT (ACE) and were not accompanied by a significant change in P_{dyn} . Also, $|B_y|$ was

large for these events so that they occurred following conditions for which convection is expected to have been quite strong. The nightside H observations for these events (HON) show positive H perturbations initiating at ~ 0640 for S1 and ~ 0820 for S2, indicating the initiation of current wedge formation. The dayside low-latitude H observations for these events are relatively constant (indicated by horizontal arrows in the BNG and LNP panels for the 0640 UT event and in the BNG and MBO panels for the 0820 UT event), consistent with the lack of variations in P_{dyn} .

[19] WIC images for S1 and S2 events are shown in Figures 6a and 6b, respectively. Auroral brightening within the expected region of the Harang reversal is first evident in the 0640:14 UT image for S1 and in the 0820:24 UT image for S2, consistent with the times of current wedge formation inferred from the nightside low-latitude H component. Also, the geosynchronous energetic particle flux for these events clearly shows the effects of nightside current wedge formation. The only significant difference from the images for typical substorms is that the region of enhanced expansion-phase aurora after onset spreads azimuthally to a maximum azimuthal coverage of ~ 6 –7 hours of MLT, which is somewhat broader than for the typical substorms. Fading of the enhanced aurora is clear by about 15 min after onset, which is perhaps a little longer after onset than for typical substorms. Also, as for typical substorms, there is no persistent auroral brightening away from the bulge region.

3.2. Dynamic Pressure Disturbances

[20] The above examples do not show large differences between northward turning substorms under moderately and

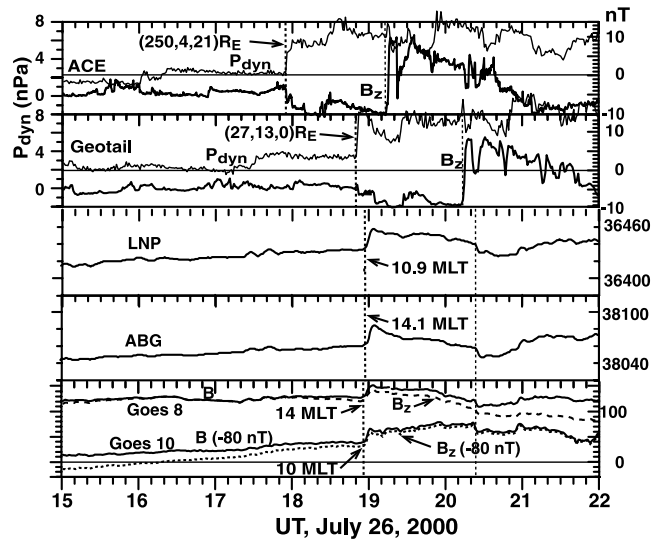


Figure 4. IMF B_z and P_{dyn} from ACE and Geotail, H-component from two dayside stations, and Goes 8 and 10 total B and B_z observations for a P_{dyn} enhancement on 26 July 2000. The GOES 10 fields are shown with 80 nT subtracted, so that they can be plotted in the same panel as the GOES 8 fields. The times of the P_{dyn} enhancement at each solar wind spacecraft and of its first effects on the ground H-component are indicated by the heavier vertical dashed line in each panel. The thinner vertical dashed line identifies a null event that occurred ~ 1.5 hours later.

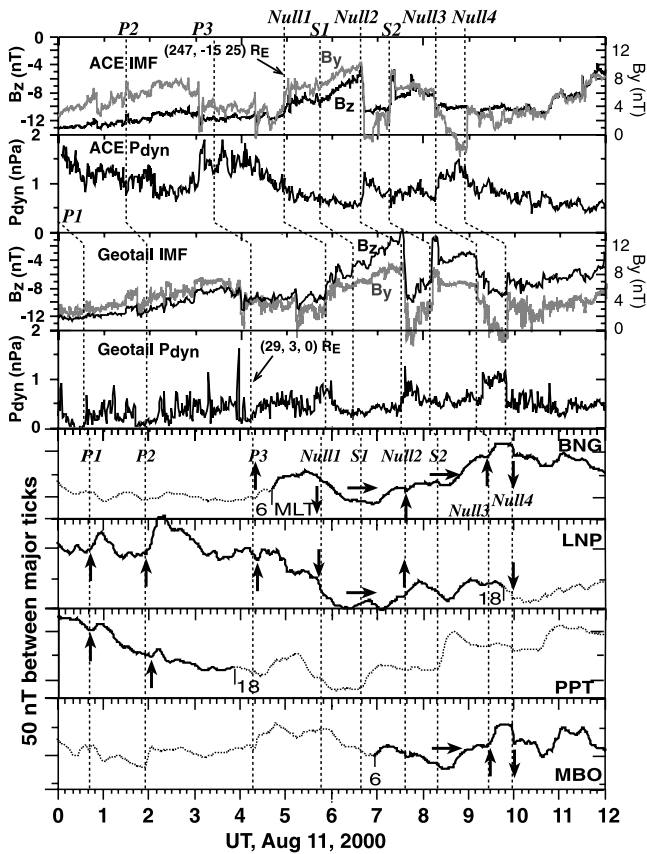


Figure 5. IMF B_z , B_z , and P_{dyn} from ACE and Geotail, and H-component from four representative low-latitude ground stations distributed in longitude for 0000–1200 UT on 11 August 2000. Vertical dashed lines identify events discussed in the text.

strongly southward IMF conditions. However, this is not the case for dynamic pressure disturbances. Three disturbances initiated by enhancements in solar wind dynamic pressure under conditions of prolonged steady strongly southward ($B_z \lesssim -10$ nT) are identified as P1, P2, and P3 in Figure 5. The impacts of these three pressure increases can be seen as increase in the dayside low-latitude H, as indicated by vertical directed arrows in the figure. (The timing of the dynamic pressure increase observed at Geotail for P2 would indicate that its impact time would be later than indicated. However, in addition to the LNP (near 1030 MLT) response shown in Figure 5, CBI (near 1200 MLT, not shown) indicates a strong pressure impact before 0200 and the LANL energetic particle data (also not shown) show strong pressure effects at ~ 0155 UT. So it seems clear that there was a significant pressure impact at ~ 0155 UT. The Geotail pressure data was highly turbulent before 0400 UT, which may have interfered with measurement of the pressure front timing at the location of Geotail.)

[21] Good WIC coverage of the auroral oval is only available for event P3, which was first evident in the low-latitude H starting near 0418 UT. Images for this event are shown in Figure 7a. Dayside imaging was not particularly good for this event because of sunlight and limitations in the

algorithm for subtracting dayglow from the images. However, some auroral brightening can be seen just to the dayside of the dawn-dusk meridian initiating in the 0415:09 and 0417:12 UT images. This is as expected from the magnetospheric compression caused by the pressure enhancement. However, simultaneously, there is a Harang region auroral brightening, which is initially seen at 2100–2300 MLT in the 0415:09 UT image and then expands azimuthally. The Harang region brightening looks essentially the same as the auroral bulge for northward turning substorms. This suggests that the pressure enhancement for this event led to formation of a substorm current wedge as well as to magnetospheric compression.

[22] The WIC observations thus show evidence for both compressive and substorm auroral enhancements for this strongly southward IMF P_{dyn} increase event. Furthermore, as the bulge-region aurora expands azimuthally, it seems to merge with the compressive auroral enhancement, particularly on the duskside. This leads to an unusually broad region of enhanced auroral emissions covering 10–14 hours of MLT by 0421:17 to 0425:22 UT. Also, clear evidence for current wedge formation within the nightside near-Earth plasma sheet, and for its occurring together with global magnetospheric compression, is seen in the geosynchronous particle data analyzed in Figure 11 in Paper 2. Evidence for fading of the bulge-region aurora at some time after onset is not as clear as for northward turning substorms, which is most likely due to the dynamic-pressure driven auroral enhancement.

[23] WIC images for another disturbance initiated by an enhancement in P_{dyn} under conditions of prolonged steady strongly southward are shown in Figures 7b. Solar wind and representative dayside low-latitude H observations for this event, on 14 October 2000, are shown in Figures 8a. The images for the event show Harang region brightening, as for the previous event, which is first discernible in the 0954:29 UT image. The solar wind observations in Figure 8a (from ACE and Geotail) show that this event was caused by a sharp increase in P_{dyn} during a period of approximately steady $B_z \sim -10$ nT. B_z changed from +2 nT to -2 nT for this event. The low-latitude H observations clearly show that the effects of the impact of the P_{dyn} increase at 0952 UT, which is just prior to when the auroral brightening was first observed. As for the first event, we see some increase in emissions somewhat to the dayside of the dawn-dusk meridian (compare the 0956:31 UT image with the 0950:24 UT image), as expected from magnetospheric compression, and the azimuthally expanding auroral bulge seems to merge with the compressive auroral enhancement to form an ~ 12 hour wide region of auroral enhancement. Again, additional evidence for near simultaneous occurrence of the substorm current wedge and the compressive responses are seen in the geosynchronous data shown in Figure 14 of Paper 2.

[24] The existence of the substorm response and its merger with the compressive response following increases in P_{dyn} during steady, strongly southward IMF conditions can readily be seen for the two events on 18 April 2002 shown in Figure 9. Unfortunately, solar wind data for this event, shown in Figure 8b is only available from ACE, which was $32 R_E$ away from the Earth-Sun line. The ACE IMF shows B_z to be steady and < -10 nT for these two

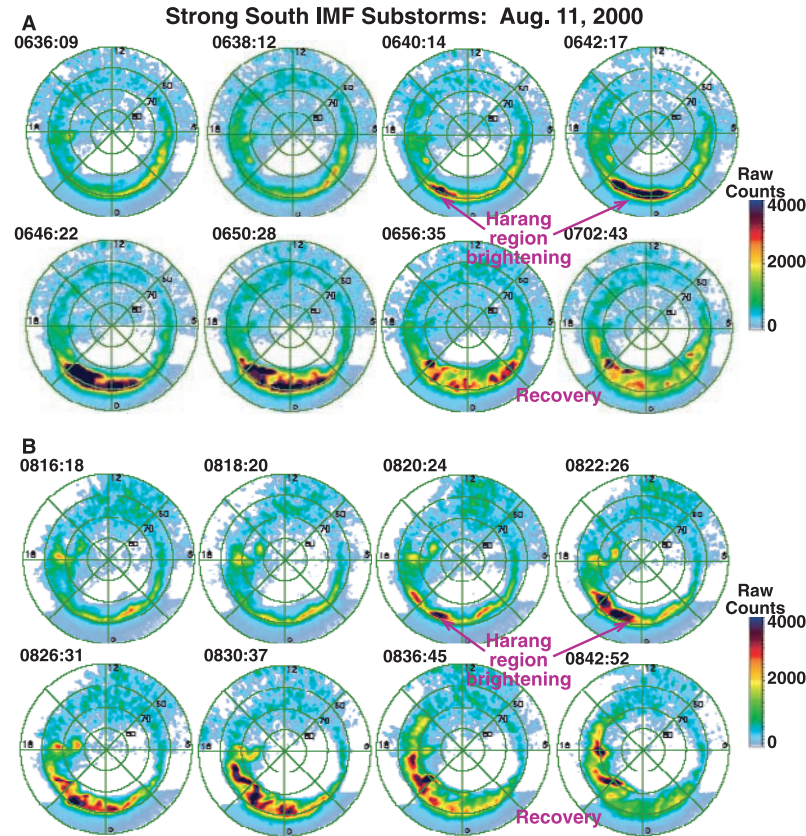


Figure 6. Selected global auroral images from WIC for northward turning substorms under strongly southward IMF conditions with onsets at ~ 0640 UT and ~ 0820 UT on 11 August 2000.

events. The pressure increases leading to these two events, identified by upward pointed arrows in the figure, are somewhat modest for these events as observed at ACE. The first event, observed at 0700 UT is nearly negligible at ACE, but the second event, while small in absolute magnitude, is much more significant and approximately doubles P_{dyn} . The smallness of the magnitude of increases in P_{dyn} observed by ACE has lead some to conclude that the disturbances during this period were not related to enhancement in P_{dyn} [e.g., Huang *et al.*, 2003]. However, the dayside low-latitude H observations for this period, shown in Figure 8b [see also Lee *et al.*, 2004], show clear positive perturbations initiating near 0806 and 1133 UT, indicating that significant increases in P_{dyn} impacted the magnetosphere at these times.

[25] The WIC images in Figure 9 show the onset of Harang region auroral brightenings in the 0808:25 UT and 1133:11 images, which correspond in time to within the image time resolution to the P_{dyn} increase impact times inferred from the low-latitude H observations. In the images 2 min earlier, afternoonside auroral enhancements are first seen. With time, these afternoonside compressive enhancement become more intense, and the auroral bulge regions expands, until the two enhancements merge (in the 0818:39 UT image for the first event and the 1143:25 UT image for the second event). This leads to disturbance-related increases in auroral emissions extending from ~ 1500 to

~ 0300 MLT. The region of strong emissions actually extends to past 0600 MLT for these events, but the morning-side emissions were already strong before the disturbances because of the strong earthward convection and dawnward magnetic drift, and thus strong energization, of plasma sheet electrons that occurs during periods of strongly enhanced convection. Thus we again see evidence for the two-mode auroral response for these events. This two-mode response can be seen in the geosynchronous particle data (not shown) for the 0808 UT event. There is not sufficient dayside geosynchronous data to examine the two-mode response for the 1133 UT event.

[26] Thus for all four events shown here, and the limited number of other events we have looked at, we see a significant difference between dynamic pressure disturbances under not-strongly-southward and under strongly southward conditions. The compressive response is seen for all events, but the substorm current wedge associated auroral enhancement is only seen for the strongly southward IMF events. Strong auroral enhancements associated with large, abrupt increases in P_{dyn} have been analyzed also by Zhou and Tsurutani [2001] and very recently by Meurant *et al.* [2005]. Zhou and Tsurutani [2001] found strong nightside auroral enhancements for events preceded by southward IMF but did not distinguish between Harang region auroral enhancements, indicative of current wedge expansion, and the compressive response. It is likely, however, that many of

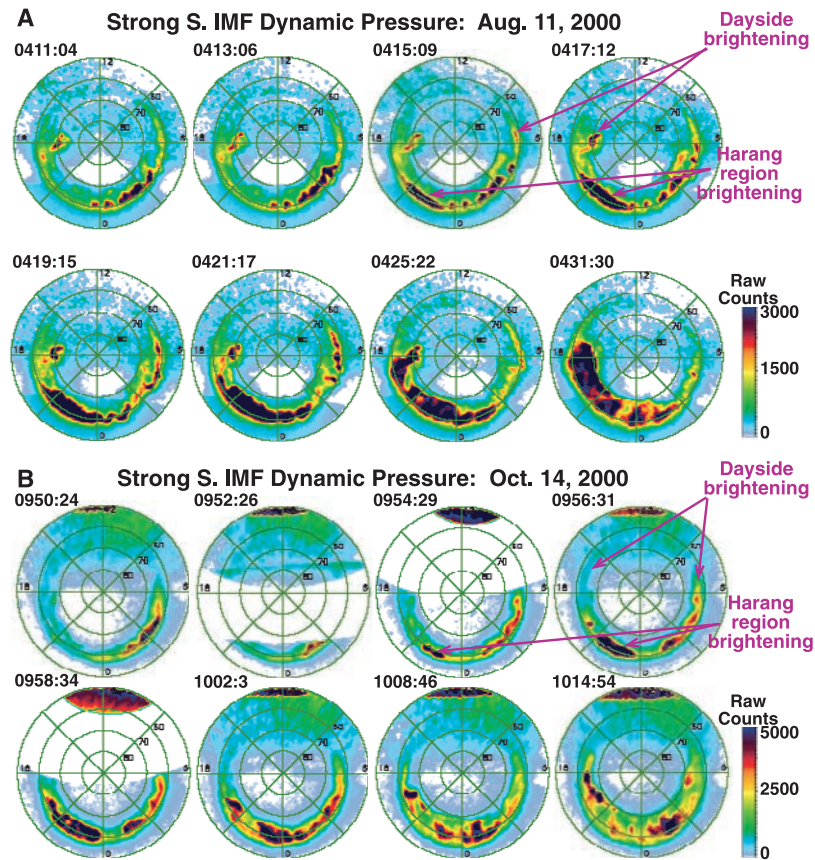


Figure 7. Selected global auroral images from WIC for dynamic pressure disturbances under strongly southward IMF conditions with onsets at ~ 0415 UT on 11 August 2000 and ~ 0954 UT on 14 October 2000.

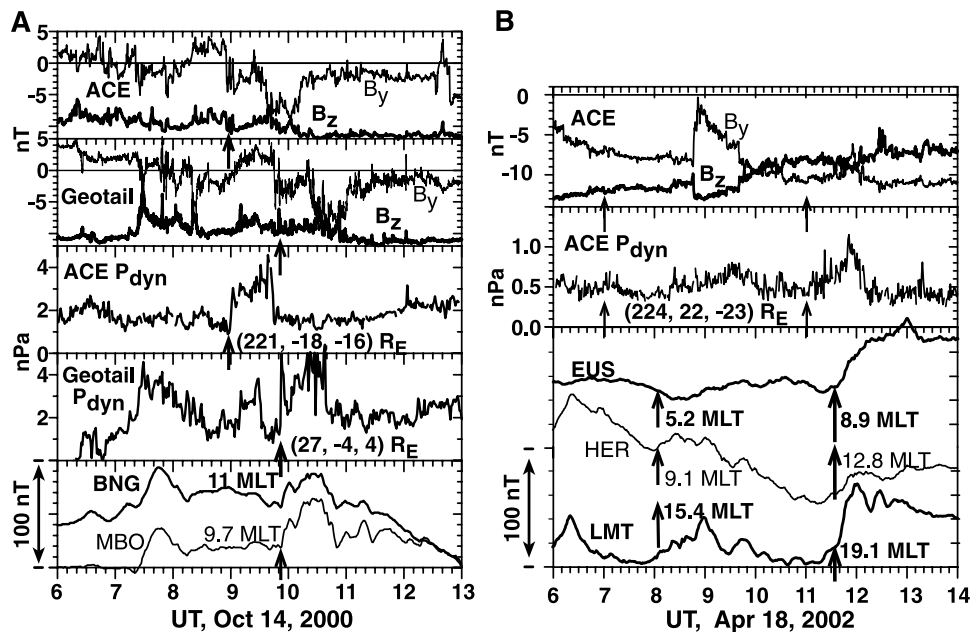


Figure 8. IMF B_y , B_z , and P_{dyn} from ACE and Geotail (8a only) and H-component from representative dayside low-latitude ground stations distributed for 0600–1300 UT on 14 October 2000 and 0600–1400 UT on 18 April 2002. Event times are indicated by vertical arrows.

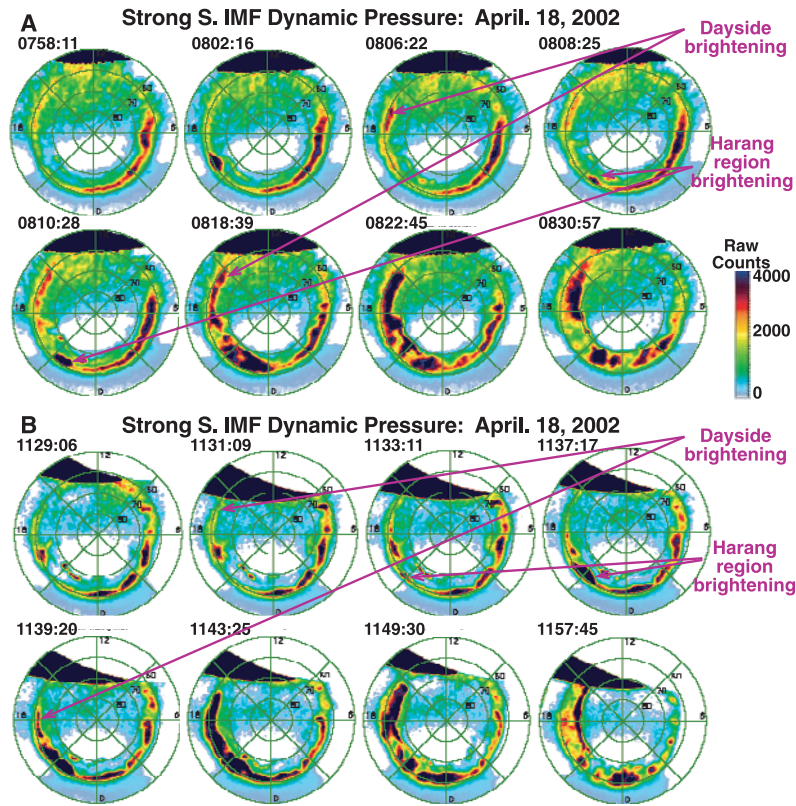


Figure 9. Selected global auroral images from WIC for dynamic pressure disturbances under strongly southward IMF conditions with onsets at ~ 0806 UT on ~ 1133 UT on 18 April 2002.

their events had the Harang region auroral response identified here so that their conclusion that abrupt increases in P_{dyn} can trigger substorms is consistent with our results. Meurant *et al.* [2005] show WIC images for one event at 0808 UT on 28 October 2000 that was associated with an abrupt increase in P_{dyn} without a concurrent northward turning. The images show a clear Harang region onset for this event. While not considered by Meurant *et al.*, the images in their paper show evidence that an afternoonside compressive response occurred as well, possibly providing an additional case supporting the two-mode auroral response to such events proposed here.

3.3. Null Events

[27] The above events were all selected because they are quite ideal in that there was either an IMF northward turning with approximately steady P_{dyn} or an increase in P_{dyn} with approximately steady IMF B_z . However, it is far more common for a solar wind change to simultaneously affect both B_z and P_{dyn} . If increases in solar wind dynamic pressure and northward turnings of the IMF can cause nightside substorm disturbances, it makes sense that effects of changes in these quantities should interact if both occur simultaneously. For example, it would seem that an IMF northward turning accompanied by an increase in P_{dyn} might lead to a stronger disturbance than would an equal change in only one of the quantities. Determining whether or not this is true would require comparison between

appropriately selected pairs of events, and such pairs have not been identified for the present study. However, we have been able to determine that there indeed is important interaction between effects of IMF B_z changes and P_{dyn} changes under strongly southward IMF conditions by considering events where P_{dyn} decreases (increases) and there is a simultaneous northward (further southward) turning of the IMF.

[28] Four such events occurred on 11 August 2000 and are identified in Figure 5 as Null1–Null4. Two of these had an IMF northward turning from $B_z < -8$ nT and a simultaneous decrease in P_{dyn} (Null1 and Null 4), which can be seen more clearly in the Geotail observations than the ACE observations. The other two events, Null2 and Null3, had a further southward IMF turning and an increase in P_{dyn} . The impacts of the P_{dyn} changes for these events are clearly seen in the low-latitude H observations shown in Figure 5, as indicated by the upward and downward pointing arrows for the increasing and decreasing P_{dyn} cases, respectively.

[29] WIC images for the Null3 and Null4 events are shown in Figure 10a and 10b, respectively. The low-latitude H data in Figure 5 show that the impacts on the magnetosphere of the solar wind changes for these events were at 0929 and 0958 UT, respectively. On the basis of the results from the previous events, we would expect that the P_{dyn} increase for Null3 and the IMF northward turning for Null4 would, by themselves, have caused a significant, large-scale

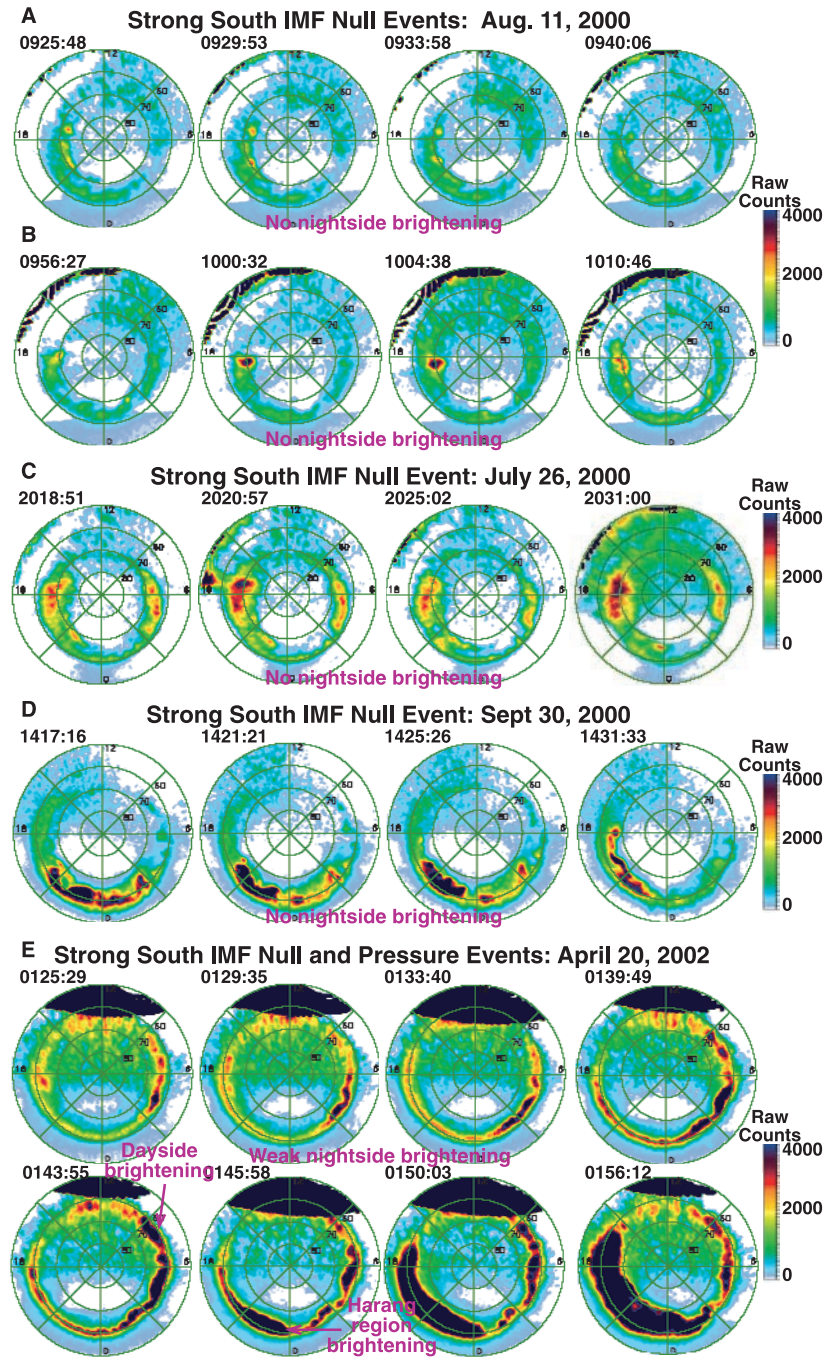


Figure 10. Selected global auroral images from WIC for null events with onsets at ~ 0929 UT and ~ 0958 UT on 11 August 2000, at 2023 UT on 26 July 2000, at 1422 UT on 30 September 2000, and at 0127 UT on 20 April 2002. Additional images for 20 April 2002 (last panels) are included to show a P_{dyn} /IMF northward turning event with onset at ~ 0144 UT.

auroral disturbance. However, the images clearly show that such a disturbance did not occur for these events. Similarly, disturbances were also not observed for the Null1 and Null2 events identified in Figure 5 (images not shown). These results for the 11 August 2000 events suggest that the effects of a P_{dyn} decrease (increase) and a simultaneous northward (further southward) turning of the IMF can

nullify each other so that a large-scale disturbance, and in particular a substorm response, does not occur.

[30] For Null2 and Null4, a Harang region substorm onset would be expected from the IMF change but did not occur. The IMF may not have been sufficiently southward for the dynamic pressure increase to cause a substorm disturbance for Null1 and Null3, but an event discussed below (on 20

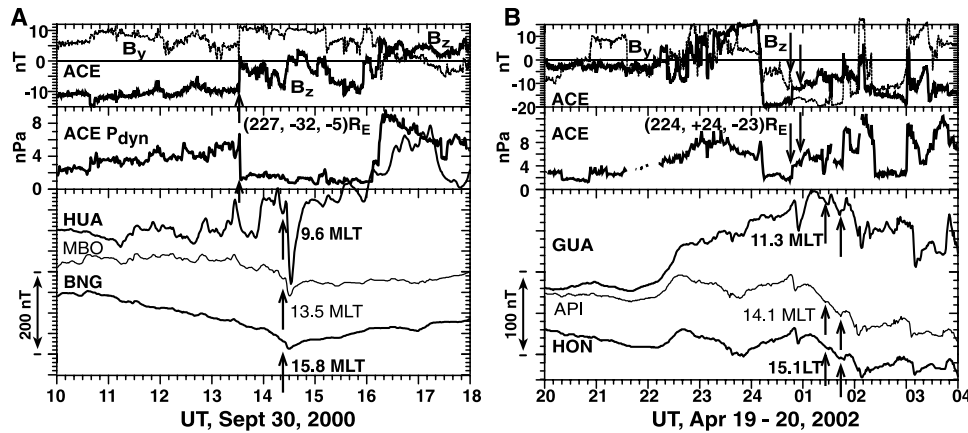


Figure 11. IMF B_y , B_z , and P_{dyn} from ACE and H-component from representative dayside low-latitude ground stations for 1000–1800 UT on 30 September 2000 and 0000–0400 UT on 18–19 April 2002. Event times are indicated by vertical arrows.

April 2002) shows that a substorm onset did not occur when the IMF was strongly southward before the dynamic pressure increase. A large-scale auroral enhancement due to the increase in P_{dyn} also was not observed for Null1 and Null3, though some increase was observed for the 20 April 2002 null event discussed below. The geosynchronous energetic particle data (not shown) also show no significant disturbances for these events; however a detailed analysis of the geosynchronous particle response to the null events is beyond the scope of Paper 2.

[31] There were IMF B_y changes for the events on 11 August 2000 that were of about the same magnitude as the B_z changes and would be expected to have had some effects on the strength of convection, though not as large as the effects due to the B_z changes. IMF B_y changes were not as large as the B_z changes for the two events for which WIC images are shown in Figures 10c and 10d. Figure 10c shows images for an event that impacted the magnetosphere at 2023 UT on 26 July 2000. Solar wind, dayside low-latitude H, and dayside geosynchronous magnetic observations for this event are shown in Figure 4, where the event is identified by the second of the two vertical dashed lines. A large, abrupt northward IMF turning was observed for this event, with B_z being -5 to -10 nT for about 1 1/2 hour prior to the northward turning. A $|B_y|$ increase of a few nT (not shown) also occurred for this event but was much less than the increase in B_z (~ 15 nT). The solar wind observations show only a modest reduction in P_{dyn} for this event. However, the low-latitude H and geosynchronous magnetic field show quite large decreases implying that the actual decrease in P_{dyn} that impacted the magnetosphere was large. The northward turning for this event would, by itself, be expected to lead to a substorm. However, as can clearly be seen from the WIC images, there is no Harang region auroral brightening for this event. Also, the low-latitude H component observations on the nightside (not shown) show decreases for this event, which indicates that current wedge formation did not occur for this event.

[32] Figure 10d shows images for a sharp northward turning accompanied by a sharp decrease in P_{dyn} that occurred following a many hour period of strongly south-

ward IMF on 30 September 2000. A $|B_y|$ increase of ~ 5 nT also occurred for this event but was significantly less than the ~ 10 nT increase in B_z . This event impacted the magnetosphere at 1422 UT (see solar wind and dayside low-latitude H data in Figure 11a). There were some preexisting eveningside auroral enhancements at the time of this event, but no substorm activity was caused by the impact of this northward turning on the magnetosphere, which is consistent with the geosynchronous particle data.

[33] The event in Figure 10e, on 20 April 2002, is interesting because there were two increases in P_{dyn} that impacted the magnetosphere at 0127 and 0142 UT (see solar wind and dayside low-latitude H data in Figure 11b) following a 30 min period of very strongly southward IMF B_z (~ -20 nT). The first was accompanied by a IMF change that include both a northward IMF turning and a very large (>10 nT) increase in $|B_y|$. There was some weak global brightening in response to the increase in P_{dyn} for this event. However the WIC images show that the increase in $|B_y|$, which would be expected to cause a significant increase in the convection electric field, was sufficient to nullify the effects of the increase in P_{dyn} and B_z and prevent a substorm onset. On the other hand, the second increase in P_{dyn} was accompanied by a small northward turning and approximately constant IMF B_y , and this event led to a large auroral disturbance, having both a dayside compressive response and a nightside Harang region substorm response that lead to auroral brightening that extended over about 18 hours in azimuth from 1500 to 0900 MLT. These two events illustrate that an increase in $|B_y|$ can lead to a null event, as has been previously noted by Blanchard *et al.* [2000], and clearly show the difference in response to increases in P_{dyn} that are accompanied by a significant increase in the convection electric field and those that are not.

4. On the Cause of IMF Substorm, Strong South IMF Pressure, and Null Events

[34] Lyons *et al.* [2003b] have presented theoretical concepts offering an explanation of how a reduction in large-scale convection imparted to the magnetosphere by an

appropriate IMF change might lead to the substorm expansion phase by causing current wedge formation, and thus auroral brightening, in the Harang reversal region. Here we show how the same concepts also offer a possible explanation for the substorm response when an increase in P_{dyn} follows a prolonged period of strongly enhanced convection and for the lack of a substorm response for the null events.

[35] The theory applies the single-species, equatorial plasma-sheet continuity equation for isotropic plasma pressure P [Heinemann, 1999]

$$\left(\frac{\partial}{\partial t} + \mathbf{V}_E \cdot \nabla\right)(n\mathcal{V}) = -\frac{\hat{\mathbf{B}}_e \cdot \nabla P \times \nabla \mathcal{V}}{qB_e} \quad (1)$$

to plasma sheet ions. Here n is ion density, \mathcal{V} is flux tube volume, \mathbf{V}_E is the electric drift velocity, q is the electronic charge, and \mathbf{B}_e is the equatorial magnetic field. When applied to the nightside plasma sheet, this equation states that the flux tube particle content $n\mathcal{V}$ at a particular location changes in response to a source from earthward electric drift and a loss, given by the term on the right-hand-side of (1), that results from particle divergence driven by the energy dependent magnetic drift.

[36] First, Lyons *et al.* [2003b] considered the response of the plasma sheet to an enhancement in convection, as occurs following a southward turning of the IMF. Since $n\mathcal{V}$ increases with radial distance, equation (1) shows that an increase in earthward directed V_E will lead to an increase in $n\mathcal{V}$ with time within the inner plasma sheet. This will lead to an increase in P within the inner plasma sheet. Because of magnetic drift and the finite width of the tail [Spence and Kivelson, 1990, 1993; Wang *et al.*, 2004], the increase in P is associated with an increase in the azimuthal component of ∇P , which is directed duskward. This, combined with the outward directed $\nabla \mathcal{V}$, increases the loss term in (1) with time. Since the loss term represents a divergence of particles, it also represents a divergence in cross-tail current, which leads to the development of the Harang electric field reversal in order to maintain current continuity in the magnetosphere and ionosphere [Erickson *et al.*, 1991]. The above responses to an enhancement in convection account for the enhancements in plasma pressure and cross-tail current [Wang *et al.*, 2004] and for the formation of the Harang reversal observed [Bristow *et al.*, 2001] during the substorm growth phase. Enhancements in the plasma pressure, cross-tail current, and Harang reversal can continue until the pressure increases sufficiently for the loss due to the magnetic-drift-driven particle divergence to balance the source due to enhanced earthward convection, in which case a steady state would be reached. On the basis of the modeling results of Wang *et al.* [2004], this could take a few hours.

[37] The theory attributes substorm expansion phase, current wedge formation to a reduction in the strength of convection within the inner plasma sheet. This reduces the source due to earthward electric drift in (1). If the magnitude of the source term is reduced to less than the magnitude of the loss term, it will lead to a reduction in $n\mathcal{V}$ and P , with the maximum rate of reduction occurring within the Harang reversal region. This leads to an azimuthally localized

maximum reduction in cross-tail current, and thus current wedge formation, within the Harang region.

[38] Lyons *et al.* [2003b] only considered a reduction in the plasma sheet electric field as a cause of current wedge formation. However, anything that reduces the source term relative to the loss term in (1) is a potential cause of current wedge formation, and the source and loss terms in (1) are functions of the equatorial electric field in the plasma sheet E and of B_e . IMF changes modify E , and the magnetopause current changes resulting from P_{dyn} changes modify B_e . Thus both IMF and P_{dyn} changes can affect the balance between the source and loss terms in (1). The source term $\mathbf{V}_E \cdot \nabla(n\mathcal{V})$ varies as $EnV/B_e L_\nabla$, where L_∇ is the scale length for spatial gradients, and the loss term given by the right-hand side of (1) varies as $PV/qB_e L_\nabla^2$. A change in B_e due to abrupt changes in P_{dyn} will give adiabatic compression, which conserves $PV^{5/3}$ and $n\mathcal{V}$. Also, Lyons *et al.* found that the T96 magnetic field model gives $\mathcal{V} \sim B_e^{-3/2}$ to B_e^{-1} . Assuming that changes in E and B_e do not lead to significant relative changes in L_∇ between the source and loss terms in (1), we find that the source term varies as E/B_e and that the loss term varies as B_e^0 to $B_e^{-1/3}$, which is nearly independent of B_e . The ratio between the source and loss terms in (1) therefore varies approximately as E/B_e . Thus an enhancement in P_{dyn} , which gives an increase in B_e throughout the magnetosphere, may decrease the source term relative to the loss term in (1), as does an IMF northward turning, which decreases E . Thus, based on this theory, increases in P_{dyn} , as well as decreases in E , can lead to current wedge formation if the increase in B_e in the inner plasma sheet is substantial relative to the preexisting B_e , and assuming that the increase in P_{dyn} does not lead to a simultaneous relative increase in E that exceeds the relative increase in B_e .

[39] Typical increases in B on the nightside in responses to increases in P_{dyn} are ~ 10 nT at synchronous orbit [e.g., Lee and Lyons, 2004]. Such an increase most often is not significant compared to B_e at synchronous orbit (which is ~ 100 nT from the Earth's dipole field). However, modeling has shown that B_e can become below 10 nT within the $r \sim 7-10 R_E$ region of the inner plasma sheet following prolonged periods of enhanced convection [Sergeev *et al.*, 1994; Wang *et al.*, 2004], and B_e values below 10 nT have been observed within this region of the plasma sheet prior to substorm onset [Lui *et al.*, 1988; Lyons *et al.*, 2003a]. Thus an increase in P_{dyn} can cause a significant increase in B_e if it occurs following a period of strongly southward IMF, when B_e is substantially reduced within the inner plasma sheet. This is particularly important because increases in P_{dyn} have been observed to cause an increase in the strength of convection [Lukianova, 2003; Boudouridis *et al.*, 2004], so that a large relative increase in B_e is necessary for an increase in P_{dyn} to reduce E/B_e and thus cause current wedge formation.

[40] This shows that an increase in P_{dyn} , as well as a decrease in E , has the potential for reducing the source term relative to the loss term in (1) and leading to substorm current wedge formation. However, qualitatively, B_e must be low in the inner plasma sheet for an increase in P_{dyn} to cause current wedge formation, which offers a possible explanation for why a substorm auroral response is observed here only for the cases following a prolonged period

of strongly southward IMF. If the above arguments are correct, we would expect that larger increases in P_{dyn} would be required for current wedge formation for higher values of B_e . Thus a larger increase in P_{dyn} would be required following less strongly southward or less prolonged periods of southward IMF than would be required following a stronger or more prolonged southward IMF. However, we are not able to test this prediction with the limited number of examples examined here.

[41] The above arguments also offer an explanation for the null events, since it is a decrease in V_E that leads to current wedge formation. An IMF change leading to a reduction in E (such as a northward turning) that occurs simultaneously with a decrease in P_{dyn} can cause a simultaneous decrease in E and B_e , which could leave V_E unchanged or increased within the inner plasma sheet. Similarly, an increase in P_{dyn} and a simultaneous IMF change that leads to an increase in E (such as a further southward turning) could leave V_E unchanged or increased. In both cases, there would not be a decrease in V_E so that current wedge formation would not be expected to occur.

5. Summary and Conclusions

[42] We have used WIC images to investigate how specific solar wind changes relate to the type, structure, and intensity of the resulting auroral-region disturbance, with the goal of determining fundamental types of responses. For this initial study, we selected only ideal solar wind changes (e.g., isolated IMF or P_{dyn} changes only) that we are quite certain impacted the magnetosphere. Confidence that impact occurred was based on multi-spacecraft or well-placed solar wind measurements, geosynchronous observations, and low-latitude ground H observations.

[43] We separated examples into those that occurred following strongly southward IMF conditions ($B_z \lesssim -10$ nT) and those that did not. For not strongly southward IMF conditions, we found that IMF changes that are expected to reduce the magnetospheric electric field (e.g., an IMF northward turning) after $\gtrsim 30$ min of negative IMF B_z cause what we have referred to as a typical substorm. These substorms have expansion phase auroral activity that initiates within the expected location of the Harang reversal and expands in ~ 10 min to cover ~ 5 hours of MLT. This auroral response and the geosynchronous energetic particle data for these events (see Paper 2) give clear evidence that substorm current wedge formation occurs within inner plasma sheet. There is no evidence for sustained expansion-phase auroral brightening away from the bulge region for these events.

[44] For not strongly southward IMF conditions, we found that solar wind dynamic pressure enhancements cause what we have referred to as a typical dynamic pressure disturbance. The pressure enhancements for these events compress the entire magnetosphere, resulting in compressive energization of plasma sheet particles and enhancement of global current systems. This leads to an enhancement of all aurora resulting from the pitch angle diffusion of plasma sheet electrons, leading to a sustained global auroral brightening. (Near noon, some of the aurora is due to direct

precipitation of magnetosheath particles along open field lines, and this precipitation will also increase when P_{dyn} increases.) There is no evidence for substorm bulge-region aurora or current wedge formation for these disturbances.

[45] The above results are consistent with much previous work and show that there is a clear distinction between the physics of substorms, which are relatively localized in MLT extent and are related to the Harang reversal, and dynamic pressure disturbances, which appear to be a direct and global consequence of compression. Following prolonged strongly southward IMF, an IMF change leading to convection reduction gives a substorm disturbance that is not very much different from the typical substorms for less strongly southward IMF conditions. The only difference we have noted is that the expansion phase auroral bulge region seems to expand somewhat more in azimuth, giving ~ 6 – 7 hours of MLT brightening. As for typical substorms, the substorm current wedge forms in the inner plasma sheet (see also Paper 2) and no sustained expansion-phase auroral brightening is observed away from bulge region.

[46] However, under steady, strongly southward IMF conditions, we have found that a solar wind dynamic pressure enhancement causes both compressive auroral brightening away from the bulge region and a Harang-region substorm auroral brightening. As the substorm bulge aurora expands in azimuth and the compressive auroral enhancement increases, the two auroral enhancements merge together leading to a very broad auroral enhancement, covering 10–15 hours of MLT. These auroral signatures imply there are both current wedge formation and compressive energization in the inner plasma sheet for these events, and energetic particles at synchronous orbit show concurrent signatures of both phenomena (see Paper 2).

[47] Furthermore, we have identified an important interplay of effects when a significant IMF change and a significant dynamic pressure change occur simultaneously. Specifically, we have found that an IMF change leading to a reduction in E (such as a northward turning), that would by itself be sufficient to cause a substorm, does not cause a substorm when it occurs simultaneously with a significant decrease in P_{dyn} . Also, an increase in P_{dyn} under strongly southward IMF conditions, that would by itself would lead to a substorm response, does not cause a substorm response when it occurs simultaneously with an IMF change that leads to a significant increase in E (such as a further southward turning). We have referred here to such events as null events. We have not, however, determined how much change in P_{dyn} and IMF is necessary to prevent a substorm response or whether a simultaneous increase in P_{dyn} and IMF change that leads to a decrease in E would cause a stronger substorm disturbance than would either one occurring separately. We plan to examine in the future the interplay between IMF and P_{dyn} changes in a more comprehensive way based on more events and more data.

[48] Finally, we argued that consideration of the plasma sheet continuity equation offers a possible explanation for the IMF and pressure driven substorm responses and for the null events. A reduction of V_E within the inner plasma sheet decreases the source term relative to the loss term, and such

a reduction has been proposed as being a cause of current wedge formation, and thus of substorm onset, within the inner plasma sheet [Lyons *et al.*, 2003b]. Lyons *et al.* considered only a reduction in E within the inner plasma sheet as a cause of substorm onset; however a significant increase in B_e , as can occur as a result of an increase in P_{dyn} , would have the same effect. For an increase in B_e resulting from an increase in P_{dyn} to be significant relative to the preexisting B_e , the preexisting B_e must be relatively small (≤ 10 nT) as only occurs following a prolonged period of enhanced convection. This could explain why increases in P_{dyn} only cause a substorm response if they occur following a prolonged period of strongly southward IMF. It should be expected that the amount of increase in P_{dyn} necessary for causing a substorm onset would depend upon B_e at the time of the P_{dyn} increase, but we have not evaluated whether or not this is the case.

[49] An IMF change leading to a reduction in E that occurs simultaneously with a decrease in P_{dyn} can cause a simultaneous decrease in E and B_e . Also an increase in P_{dyn} and a simultaneous IMF change that leads to an increase in E can cause a simultaneous increase in E and B_e . Either could leave V_E unchanged or increased within the inner plasma sheet, so that current wedge formation would not be expected to occur. This offers a possible explanation for the null events. Whether or not a null event or a substorm will occur following a specific change in IMF and P_{dyn} should depend upon the resulting change in V_E , which depends upon the pre-existing values of, and the changes in E and B_e . It should be interesting to test this possibility in the future.

[50] **Acknowledgments.** This research was supported at UCLA in part by NSF grants OPP-0136139 and ATM-0207298. The work at Chungbuk National University was supported by grant R01-2002-000-00100-0 from Basic Research Program of the Korea Science and Engineering Foundation. We are grateful to Harald Frey for assistance in understanding the analysis of the WIC images and to Thomas Immel for his help in getting the FUV imager software running at UCLA. The solar wind plasma and magnetic field data of ACE, Wind, and Geotail used here were obtained from NASA's CDAWeb site, and we are grateful to each of the principal investigators, D. J. McComas, N. Ness, K. Ogilvie, R. Lepping, L. Frank, and S. Kokubun. The geomagnetic data used were obtained from WDC at Copenhagen.

[51] Arthur Richmond thanks Renata Lukianova and another reviewer for their assistance in evaluating this paper.

References

- Arnoldy, R. L., and T. E. Moore (1983), Longitudinal structure of substorm injections at synchronous orbit, *J. Geophys. Res.*, **88**, 6213.
- Baumjohann, W. J., Pellinen, H. J. Opgenoorth, and E. Nielsen (1981), Joint two-dimensional observations of ground magnetic and ionospheric electric fields associated with auroral zone currents: Current systems associated with local auroral break-ups, *Planet. Space Sci.*, **29**, 431.
- Blanchard, G. T., L. R. Lyons, and J. Spann (2000), Predictions of substorms following northward turnings of the IMF, *J. Geophys. Res.*, **105**, 375.
- Boudouridis, A., E. Zesta, R. Lyons, P. C. Anderson, and D. Lummerzheim (2003), Effect of solar wind pressure pulses on the size and strength of the auroral oval, *J. Geophys. Res.*, **108**(A4), 8012, doi:10.1029/2002JA009373.
- Boudouridis, A., E. Zesta, L. R. Lyons, P. C. Anderson, and D. Lummerzheim (2004), Magnetospheric reconnection driven by solar wind pressure fronts, *Ann. Geophys.*, **22**, 1367.
- Bristow, W. A., A. Otto, and D. Lummerzheim (2001), Substorm convection patterns observed by the Super Dual Auroral Radar Network, *J. Geophys. Res.*, **106**, 24,593.
- Chua, D., G. Parks, M. Brittner, W. Peria, G. Germany, J. Spann, and C. Carlson (2001), Energy characteristics of auroral electron precipitation: A comparison of substorms and pressure pulse related auroral activity, *J. Geophys. Res.*, **106**, 5945.
- Erickson, G. M., R. W. Spiro, and R. A. Wolf (1991), The physics of the Harang discontinuity, *J. Geophys. Res.*, **96**, 1633.
- Gelpi, C., H. J. Singer, and W. J. Hughes (1987), A comparison of magnetic signatures and DMSP auroral images at substorm onset: Three case studies, *J. Geophys. Res.*, **92**, 2447.
- Gjerloev, J. W., R. A. Hoffman, E. Tanskanen, M. Friel, L. A. Frank, and J. B. Sigwarth (2003), Auroral electrojet configuration during substorm growth phase, *Geophys. Res. Lett.*, **30**(18), 1927, doi:10.1029/2003GL017851.
- Heinemann, M. (1999), Role of collisionless heat flux in magnetospheric convection, *J. Geophys. Res.*, **104**, 28,397.
- Hsu, T.-S., and R. L. McPherron (2002), An evaluation of the statistical significance of the association between northward turnings of the interplanetary magnetic field and substorm expansion onsets, *J. Geophys. Res.*, **107**(A11), 1398, doi:10.1029/2000JA000125.
- Hsu, T.-S., and R. L. McPherron (2003), Occurrence frequencies of IMF triggered and nontriggered substorms, *J. Geophys. Res.*, **108**(A7), 1307, doi:10.1029/2002JA009442.
- Huang, C.-S., G. D. Reeves, J. E. Borovsky, R. M. Skoug, Z. Y. Pu, and G. Le (2003), Periodic magnetospheric substorms and their relationship with solar wind variations, *J. Geophys. Res.*, **108**(A6), 1255, doi:10.1029/2002JA009704.
- Hughes, J. M., and W. A. Bristow (2003), SuperDARN observations of the Harang discontinuity during steady magnetospheric convection, *J. Geophys. Res.*, **108**(A5), 1185, doi:10.1029/2002JA009681.
- Lee, D.-Y., and L. R. Lyons (2004), Geosynchronous magnetic field response to solar wind dynamic pressure pulse, *J. Geophys. Res.*, **109**, A04201, doi:10.1029/2003JA010076.
- Lee, D.-Y., L. R. Lyons, and K. Yumoto (2004), Sawtooth oscillations directly driven by solar wind dynamic pressure enhancements, *J. Geophys. Res.*, **109**, A04202, doi:10.1029/2003JA010246.
- Lee, D.-Y., L. R. Lyons, and G. D. Reeves (2005), Comparison of geosynchronous energetic particle flux responses to solar wind dynamic pressure enhancements and substorms, *J. Geophys. Res.*, doi:10.1029/2005JA011091, in press.
- Lui, A. T. Y., et al. (1988), A case study of magnetotail current disruption and diversion, *Geophys. Res. Lett.*, **15**, 721.
- Lukianova, R. (2003), Magnetospheric response to sudden changes in solar wind dynamic pressure inferred from polar cap index, *J. Geophys. Res.*, **108**(A12), 1428, doi:10.1029/2002JA009790.
- Lyons, L. R., G. T. Blanchard, J. C. Samson, R. P. Lepping, T. Yamamoto, and T. Moretto (1997), Coordinated observations demonstrating external substorm triggering, *J. Geophys. Res.*, **102**, 27,039.
- Lyons, L. R., E. Zesta, J. C. Samson, and G. D. Reeves (2000), Auroral disturbances during the January 10, 1997 magnetic storm, *Geophys. Res. Lett.*, **27**, 3237.
- Lyons, L. R., S. Liu, J. M. Ruohoniemi, S. I. Solov'yev, and J. C. Samson (2003a), Observations of dayside convection reduction leading to substorm onset, *J. Geophys. Res.*, **108**(A3), 1119, doi:10.1029/2002JA009670.
- Lyons, L. R., C.-P. Wang, and T. Nagai (2003b), Substorm onset by plasma sheet divergence, *J. Geophys. Res.*, **108**(A12), 1427, doi:10.1029/2003JA010178.
- Meurant, M., J.-C. Gérard, C. Blockx, V. Coumans, B. Hubert, M. Connors, and L. R. Lyons (2005), Comparison of intense nightside shock-induced precipitation and substorm activity, *J. Geophys. Res.*, **110**, A07228, doi:10.1029/2004JA010916.
- Nagai, T. (1987), Field-aligned currents associated with substorms in the vicinity of synchronous orbit: 2. Geos 2 and Geos 3 observations, *J. Geophys. Res.*, **92**, 2432.
- Nielsen, E. (1991), Ionosphere-magnetosphere mapping of dynamic auroral structures during substorms, in *Auroral Physics*, edited by C.-I. Meng and M. J. Rycroft, p. 409, Cambridge Univ. Press, New York.
- Nielsen, E., and R. A. Greenwald (1978), Variations in ionospheric currents and electric fields in association with absorption spikes during the substorm expansion phase, *J. Geophys. Res.*, **83**, 5645.
- Sergeev, V. A., T. I. Pulkkinen, R. J. Pellinen, and N. A. Tsyganenko (1994), Hybrid state of the tail magnetic configuration during steady convection events, *J. Geophys. Res.*, **99**, 23,571.
- Spence, H. E., and M. G. Kivelson (1990), The Variation of the plasma sheet polytropic index along the midnight meridian a finite width magnetotail, *Geophys. Res. Lett.*, **17**, 591.
- Spence, H. E., and M. G. Kivelson (1993), Contributions of the low-latitude boundary layer to the finite width magnetotail convection model, *J. Geophys. Res.*, **98**, 15,487.
- Tsurutani, B. T., X.-Y. Zhou, and W. D. Gonzalez (2004), A lack of substorm expansion phases during magnetic storms induced by magnetic

- clouds?, in *Disturbances in Geospace: The Storm-Substorm Relationship*, *Geophys. Monogr. Ser.*, vol. 142, edited by A. S. Sharma, Y. Kamide, and G. S. Lakhina, p. 23, AGU, Washington, D. C.
- Wang, C.-P., L. R. Lyons, M. W. Chen, and F. R. Toffoletto (2004), Modeling the transition of the inner plasma sheet from weak to enhanced convection, *J. Geophys. Res.*, *109*, A12202, doi:10.1029/2004JA010591.
- Zesta, E., H. J. Singer, D. Lummerzheim, C. T. Russell, L. R. Lyons, M. J. Brittnacher (2000), The effect of the January 10, 1997 pressure pulse on the magnetosphere-ionosphere current system, in *Magnetospheric Current Systems*, edited by S. Ohtani and R. L. Lysak, p. 217, AGU, Washington, D. C.
- Zhou, X.-Y., and B. T. Tsurutani (2001), Interplanetary shock triggering of nightside geomagnetic activity: Substorms, pseudobreakups, and quiescent events, *J. Geophys. Res.*, *106*, 18,957.
- Zhou, X. Y., et al. (2003), Ring current intensification and convection-driven negative bays: Multisatellite studies, *J. Geophys. Res.*, *108*(A11), 1407, doi:10.1029/2003JA009881.
-
- D.-Y. Lee, Department of Astronomy and Space Science, College of Natural Sciences and Institute for Basic Science Research, Chungbuk National University, 48 Gaeshin-dong, Heungduk-gu, Cheongju, Chungbuk 361-763, South Korea. (dylee@chungbuk.ac.kr)
- L. R. Lyons and C.-P. Wang, Department of Atmospheric and Oceanic Sciences, University of California, Los Angeles, CA 90095-1565, USA. (larry@atmos.ucla.edu; cat@atmos.ucla.edu)
- S. B. Mende, Space Sciences Laboratory, University of California, Berkeley, 7 Gauss Way, Berkeley, CA 94720-7450, USA. (mende@ssl.berkeley.edu)